

**Measurements of  
energy and water  
vapor fluxes in the  
Heihe River Basin**

S. Liu et al.

This discussion paper is/has been under review for the journal Hydrology and Earth System Sciences (HESS). Please refer to the corresponding final paper in HESS if available.

# Measurements of energy and water vapor fluxes over different surfaces in the Heihe River Basin, China

S. Liu<sup>1</sup>, Z. Xu<sup>1</sup>, W. Wang<sup>2</sup>, J. Bai<sup>1</sup>, Z. Jia<sup>1</sup>, M. Zhu<sup>1</sup>, and J. Wang<sup>2</sup>

<sup>1</sup>State key laboratory of Remote Sensing Science, School of Geography, Beijing Normal University, Beijing, 100875, China

<sup>2</sup>Cold and Arid Regions Environmental and Engineering Research Institute, Chinese Academy of Sciences, Lanzhou, 730000, China

Received: 20 October 2010 – Accepted: 25 October 2010 – Published: 4 November 2010

Correspondence to: S. Liu (smliu@bnu.edu.cn)

Published by Copernicus Publications on behalf of the European Geosciences Union.

Title Page

Abstract

Introduction

Conclusions

References

Tables

Figures

⏪

⏩

◀

▶

Back

Close

Full Screen / Esc

Printer-friendly Version

Interactive Discussion

## Abstract

We analyzed the seasonal variations of energy and water vapor fluxes over three different surfaces: irrigated cropland (Yingke, YK), alpine meadow (A'rou, AR), and spruce forest (Guantan, GT). The energy and water vapor fluxes were measured using eddy covariance systems (EC) and a large aperture scintillometer (LAS) in the Heihe River Basin, China, in 2008 and 2009. We also determined the source areas of the EC and LAS measurements with a footprint model for each site, and discussed the differences between the sensible heat fluxes measured by EC and LAS. The results show that the main EC source areas were within a radius of 250 m at all sites. The main source area for the LAS (with a path length of 2390 m) stretched along a path line approximately 2000 m long and 700 m wide. The surface characteristics in the source areas changed according to season and site, and there were characteristic seasonal variations in the energy and water vapor fluxes at all sites. The sensible heat flux was the main term of the energy budget during the dormant season. During the growing season, however, the latent heat flux dominated the energy budget, and an obvious “oasis effect” was observed at YK. The evapotranspiration (ET) at YK was larger than those at the other two sites. The monthly ET reached its peak in July at YK and in June at GT in both 2008 and 2009, while it reached its peak in August at AR in 2008 and in June in 2009. The sensible heat fluxes measured by LAS at AR were larger than those measured by EC at the same site. This difference seems to be caused by the energy imbalance of EC, the heterogeneity of the underlying surfaces, and the difference between the source areas of the LAS and EC measurements.

## Measurements of energy and water vapor fluxes in the Heihe River Basin

S. Liu et al.

Title Page

Abstract

Introduction

Conclusions

References

Tables

Figures



Back

Close

Full Screen / Esc

Printer-friendly Version

Interactive Discussion



## 1 Introduction

Energy and water vapor interactions between land surfaces and the atmosphere are the most crucial ecological processes in terrestrial ecosystems (Baldocchi et al., 1997). These interactions determine convection; the long-range transport of heat, humidity and pollutants; the growth rate; and the properties of the planetary boundary layer (Wilson et al., 2000). About 70% of precipitation returns to the atmosphere through water vapor exchange (evapotranspiration, ET) at the global scale (Rosenberg et al., 1983), this proportion should be higher in arid and semi-arid regions. The temporal and spatial variations in ET can result in changes in land cover, land use, and climate (Milly et al., 2001; Gordon et al., 2003). Therefore, the quantitative estimation of energy and water vapor, especially ET in different ecosystems, is extremely important for the appropriate use of water resources and eco-environmental protection.

The eddy covariance method (EC) has been widely applied to measure the exchange of water vapor, energy, and carbon dioxide between the earth's surface and atmosphere. Nowadays, this technique is considered a standard method for measuring surface fluxes (Aubinet et al., 2000). Many papers have been published that use the EC system to measure energy and water vapor fluxes in a variety of ecosystems, including forests (Wilson et al., 2000), grasslands (Wever et al., 2002) and farmlands (Suyker et al., 2008). Nevertheless, the EC method has limitations. Reliable measurements are restricted by many factors, such as complex conditions (e.g., topography and unfavorable weather), and corrections need to be applied when processing the turbulence data (Finnigan et al., 2003). Hammerle et al. (2007) and Hiller et al. (2008) successfully deployed the EC method under such complex conditions with rigorous data processing. However, Mauder et al. (2007a) documented that different data processing schemes can lead to errors of 10–15%. In addition, one of the most important problems is the “energy imbalance” in applying the EC data to the energy budget. Wilson et al. (2002) discussed this issue and summarized the causes of the imbalance as follows: (i) a mismatch in source areas for the energy budget terms; (ii) a systematic

# HESSD

7, 8741–8780, 2010

## Measurements of energy and water vapor fluxes in the Heihe River Basin

S. Liu et al.

Title Page

Abstract

Introduction

Conclusions

References

Tables

Figures



Back

Close

Full Screen / Esc

Printer-friendly Version

Interactive Discussion



bias in instrumentation; (iii) a failure to consider energy sinks; (iv) a loss of low- and/or high-frequency contributions to turbulent fluxes; and (v) a failure to consider the advection effect. Several scientists (e.g., Cava et al., 2008; Foken, 2008) have recently grouped these causes into three main categories: (i) errors associated with measurement processes; (ii) errors associated with different scales or layers; and (iii) errors produced by a loss of low- and/or high-frequency contributions to the energy transport. Von Randow et al. (2008) emphasized that the contribution of low-frequency eddies to the energy transport, these eddies that were not “captured by the EC”, may be the main reason for the energy imbalance. Many scientists have also used the large-eddy simulation (LES) model to study the imbalance problem. This method gives us a better understanding of the physical processes that lead to fluxes on scales at which conventional single EC tower measurements are unable to detect, and the imbalances were attributed to turbulent organized structures (TOS) (Kanda et al., 2004; Steinfeld et al., 2007).

In addition to the EC system above, the large aperture scintillometer (LAS) has been widely used to measure turbulent fluxes for the last few decades, and reliable results have been obtained for both homogeneous and heterogeneous underlying surfaces (Hoedjes et al., 2002; Meijninger et al., 2002a). LAS can obtain the area averaged sensible heat flux, and the area averaged ET can be derived from the energy balance equation if the surface available energy (net radiation minus soil heat flux) is known (Meijninger et al., 2002b). Since the scintillometer’s path lengths are comparable to the pixel size of satellite images, it has broad applications (McAneney et al., 1995). However, LAS also has its limitations, such as meteorological limitations in long-term operations, including precipitation, poor visibility, and weak turbulence, and methodological limitations such as signal saturation, inner-scale dependence of the signal, and tower vibrations (Moene et al., 2009). Thus, data processing must be carried out carefully, especially in complex conditions (Meijninger et al., 2002a).

The Heihe River Basin is located in the arid and semi-arid regions of Northwest China, with the unique landscape of “ice/frozen soil-forest-river and

## Measurements of energy and water vapor fluxes in the Heihe River Basin

S. Liu et al.

[Title Page](#)[Abstract](#)[Introduction](#)[Conclusions](#)[References](#)[Tables](#)[Figures](#)[⏪](#)[⏩](#)[◀](#)[▶](#)[Back](#)[Close](#)[Full Screen / Esc](#)[Printer-friendly Version](#)[Interactive Discussion](#)

wetland-oasis-desert” which are connected by water. As an important component of the project “Watershed Airborne Telemetry Experimental Research (WATER)” (Li et al., 2009), many observation sites were established in late 2007 to measure surface fluxes of energy, momentum, and water vapor on various land surfaces to better understand the characteristics of surface-atmosphere exchange, and to develop, improve and validate land surface and hydrological models.

The main objectives of this paper are (1) to analyze the spatial representativeness of flux measurements by EC and LAS over different surfaces; (2) to study the seasonal variation characteristics of energy and water vapor fluxes over different surfaces; and (3) to compare sensible heat fluxes derived from LAS and EC.

## 2 Materials and methods

### 2.1 Site description and instrument

Our study was conducted in the Heihe River Basin, and three sites were selected: Yingke (YK, 100°24′37″ E, 38°51′26″ N; 1519 m), A’rou (AR, 100°27′53″ E, 38°02′40″ N; 3033 m), and Guantan (GT, 100°15′8″ E, 38°32′1″ N; 2835 m). The three sites represent the different kinds of climate and land cover that characterize the Heihe River Basin (Fig. 1). The YK site is located in the middle reaches of the Heihe River Basin, with an average annual air temperature and precipitation of 7.2 °C and 128.1 mm (1951–2005), respectively; The GT site is also located in the middle reaches of the Heihe River Basin, and the average annual air temperature and precipitation here are 3.3 °C and 337.1 mm (1958–2003), respectively. The AR site is located in the upper reaches of the Heihe River Basin, and it has average annual air temperatures of approximately 1 °C and an annual precipitation of 403.5 mm (1951–2005). The soil texture is a silt loam at YK, sand mixed with silt at AR, and sand with moss covering the surface at GT. YK is located in the Yingke irrigated fields, which have maize interplanted with spring wheat from May to July and maize as the sole crop from August to September

## Measurements of energy and water vapor fluxes in the Heihe River Basin

S. Liu et al.

Title Page

Abstract

Introduction

Conclusions

References

Tables

Figures



Back

Close

Full Screen / Esc

Printer-friendly Version

Interactive Discussion







the Bowen ratio closure method (Twine et al., 2000) on a daily basis. The corrected fluxes were only used to analyze the seasonal variations of ET at the three sites.

In long-term observations, missing data will occur due to instrument malfunction, maintenance, and bad weather conditions. The gap-filling methods of a look-up table (LUT) and mean diurnal variations (MDV) (Falge et al., 2001) were used to fill the flux measurement gaps. The LUT method was applied when the meteorological observation data were complete during the corresponding period; otherwise the MDV method was used. The gap-filling data were used only to analyze the seasonal variations of ET.

## 2.2.2 Large aperture scintillometer

The large aperture scintillometer consists of a transmitter and a receiver. The transmitter emits electromagnetic radiation that is scattered by the turbulent atmosphere over a distance of a few kilometers. The structure parameter of the refractive index of air,  $C_n^2$  ( $\text{m}^{-2/3}$ ), is calculated from the variance of the natural logarithm of intensity fluctuations ( $\sigma_{\ln I}^2$ ) (Wang et al., 1978)

$$C_n^2 = 1.12 \sigma_{\ln I}^2 D^{7/3} L^{-3} \quad (1)$$

where  $D$  is the aperture diameter (m), and  $L$  is the path length (m). Strictly speaking,  $C_n^2$  is related to the temperature structure parameter  $C_T^2$  ( $\text{K}^2 \text{m}^{-2/3}$ ), the humidity structure parameter  $C_q^2$  ( $\text{kg}^2 \text{m}^{-6} \text{m}^{-2/3}$ ), and a covariant term  $C_{Tq}$ . The optical scintillometer is more sensitive to variations of temperature than humidity. As a simplification, Wesely (1976) showed that  $C_n^2$  could be related to  $C_T^2$  by

$$C_T^2 = C_n^2 \left( \frac{T^2}{-7.87 \times 10^{-7} P} \right)^2 \left( 1 + \frac{0.03}{\beta} \right)^{-2} \quad (2)$$

where  $T$  is the air temperature (K),  $P$  is the air pressure (Pa), and  $\beta$  is the Bowen ratio. According to the Monin-Obukhov similarity theory (MOST), the sensible heat flux  $H_{\text{LAS}}$

## Measurements of energy and water vapor fluxes in the Heihe River Basin

S. Liu et al.

Title Page

Abstract

Introduction

Conclusions

References

Tables

Figures

⏪

⏩

◀

▶

Back

Close

Full Screen / Esc

Printer-friendly Version

Interactive Discussion



( $W m^{-2}$ ) can be calculated from the following equations:

$$\frac{C_T^2(z_{LAS} - d)^{2/3}}{T_*^2} = f_T \left( \frac{z_{LAS} - d}{L_{MO}} \right) \quad (3)$$

$$H_{LAS} = \rho_a C_p u_* T_* \quad (4)$$

$$u_* = \frac{k_v u}{\ln\left(\frac{z_u - d}{z_{0m}}\right) - \Psi_m\left(\frac{z_u - d}{L_{MO}}\right) + \Psi_m\left(\frac{z_{0m}}{L_{MO}}\right)} \quad (5)$$

5 where  $z_{LAS}$  is the effective height of LAS (m),  $d$  is the zero-plane displacement height (m),  $L_{MO}$  is the Monin-Obukhov length (m), and  $f_T$  is the stability function, defined as follows (Andreas, 1988): for unstable conditions (i.e.,  $L_{MO} < 0$ ),  $f_T = 4.9 \left[ 1 - 6.1 \left( \frac{z_{LAS} - d}{L_{MO}} \right) \right]^{-2/3}$ ; for stable conditions (i.e.,  $L_{MO} > 0$ ),  $f_T = 4.9 \left[ 1 + 2.2 \left( \frac{z_{LAS} - d}{L_{MO}} \right)^{2/3} \right]$ .  $C_p$  is the specific heat capacity of air at constant pressure ( $J kg^{-1} K^{-1}$ ),  $\rho_a$  is the density of air ( $kg m^{-3}$ ),  $u_*$  is the friction velocity ( $m s^{-1}$ ),  $T_*$  is the temperature scale (K),  $k_v$  is the von Kármán constant (0.40),  $u$  is the wind speed ( $m s^{-1}$ ),  $z_u$  is the measurement height of the wind speed (m),  $z_{0m}$  is the aerodynamic roughness length (m) and  $\Psi_m$  is the stability correction function for the momentum transfer (Paulson, 1970; Webb, 1970; Businger et al., 1971). The zero-plane displacement height is calculated by means of a simple relationship between  $d$  and the vegetation canopy height  $h_c$  (i.e.  $d = \frac{2}{3} h_c$ ), and the aerodynamic roughness length is calculated with EC data based on the method suggested by Yang et al. (2003).

15 Four steps were taken to ensure the LAS data quality. (1) Data beyond the saturation criterion of  $C_n^2$  were rejected. The saturation criterion was determined according to Ochs and Wilson (1993). The upper limit of  $C_n^2$  saturation at AR was  $7.25 \times 10^{-14} m^{-2/3}$ . (2) Data obtained during periods of precipitation were rejected.

**Measurements of energy and water vapor fluxes in the Heihe River Basin**

S. Liu et al.

Title Page

Abstract

Introduction

Conclusions

References

Tables

Figures

⏪

⏩

◀

▶

Back

Close

Full Screen / Esc

Printer-friendly Version

Interactive Discussion



(3) Data were rejected when the minimum value of the demodulated signal ( $X$ ) was less than 50 in the raw data (1 min average time period). (4) Data were rejected when the sensor was malfunctioning.

Because the scintillometer can only observe the intensity of atmosphere turbulence, it cannot determine the direction of the sensible heat flux. Thus, the difference of air temperature at two layers (namely 2 m and 10 m at AR) was used to judge the sign of the LAS flux.

After the sensible heat was calculated, the latent heat flux (evapotranspiration, ET) could be estimated from the energy balance equation using the measurements of net radiation and soil heat flux (Meijninger et al., 2002b).

$$LE_{LAS} = R_n - G_0 - H_{LAS} \quad (6)$$

where  $LE_{LAS}$  ( $W m^{-2}$ ) is the latent heat flux estimated by LAS,  $R_n$  ( $W m^{-2}$ ) is the net radiation, and  $G_0$  ( $W m^{-2}$ ) is the soil surface heat flux.

The nonlinear regression method was used to fill the 30-min missing data, and the dynamic linear regression method was used to fill the daily missing data (Alavi et al., 2006). The gap-filling data were only used to analyze the seasonal variations of ET.

### 2.2.3 Soil surface heat flux

The soil surface heat flux is an important component of the surface energy budget. Because the soil heat flux plate is usually buried within the soil, corrections were made to derive the soil surface heat flux. We used the method proposed by Yang and Wang (2008), which is a temperature prediction-correction method based on the thermal exchange equation using the profile of soil temperature and moisture observations.

$$G_z = G(z_r) + \int_{z_r}^z \frac{\partial C_v T(z)}{\partial t} dz \quad (7)$$

where  $G_z$  is the soil heat flux ( $W m^{-2}$ ) at depth  $z$ ,  $t$  is the time (s),  $C_v$  is the soil heat capacity ( $J kg^{-1} K^{-1}$ ),  $T$  is the soil temperature (K), and  $z$  is the soil depth (m) (positive

## Measurements of energy and water vapor fluxes in the Heihe River Basin

S. Liu et al.

Title Page

Abstract

Introduction

Conclusions

References

Tables

Figures

⏪

⏩

◀

▶

Back

Close

Full Screen / Esc

Printer-friendly Version

Interactive Discussion



downward), and  $G(z_r)$  is the soil heat flux at reference depth  $z_r$ . In this study, the reference depth  $z_r$  was 1.6, 1.6, and 1.2 m depth at YK, AR and GT, respectively. Therefore, we assumed  $G(z_r) \approx 0$ .

Given the temperature profile  $T(z_j)$ , the soil surface heat flux  $G_0$  is:

$$G_0 = \frac{1}{\Delta t} \sum_{z_r}^0 [c_v(z_j, t + \Delta t)T(z_j, t + \Delta t) - c_v(z_j, t)T(z_j, t)] \Delta z \quad (8)$$

where  $z_j$  is the soil depth at a certain layer  $i$  (m),  $\Delta t$  is the change in time (s), and  $\Delta z$  is the thickness of a thin layer of the soil (m).

This method constructed the soil temperature profile and then corrected it using the measured soil temperature. Integrating Eq. (8), from the bottom to the surface, one can obtain the soil surface heat flux. Table 1 lists the measurements of soil temperature and moisture profile in this study. The surface temperature ( $T_s$ ) was calculated from measurements of longwave radiation fluxes, i.e.,  $T_s = \left( \frac{R_{L\uparrow} - (1-\varepsilon)R_{L\downarrow}}{\varepsilon\sigma} \right)^{1/4}$ , where the Stefan-Boltzmann constant  $\sigma = 5.67 \times 10^{-8} \text{ W m}^{-2} \text{ K}^{-4}$ , and  $R_{L\uparrow}$  ( $\text{W m}^{-2}$ ) and  $R_{L\downarrow}$  ( $\text{W m}^{-2}$ ) are the upwards and downward longwave radiation components, respectively. The surface emissivity  $\varepsilon$  was given empirically (0.987 at YK and AR, 0.993 at GT) (Wang et al., 2008).

## 2.2.4 Footprint model

The turbulent fluxes obtained from the EC and LAS measurements reflect the influence of the underlying surface on the turbulent exchange (Schmid, 2002). The field of view of these measurements can be well-defined by the so-called source area, the sizes and extent of which depend on many factors, such as the measurement height, atmospheric stability, wind speed and direction, and surface roughness length, etc. It is necessary to determine the source area of the EC and LAS measurements using the footprint model before analyzing the characteristics of the energy and water vapor fluxes.

## Measurements of energy and water vapor fluxes in the Heihe River Basin

S. Liu et al.

Title Page

Abstract

Introduction

Conclusions

References

Tables

Figures

⏪

⏩

◀

▶

Back

Close

Full Screen / Esc

Printer-friendly Version

Interactive Discussion



In this study, we used an Eulerian analytic flux footprint model (Kormann and Meixner, 2001) to obtain the flux footprint of a single point vertical flux measurement  $f(x, y, z_m)$

$$f(x, y, z_m) = D_y(x, y) f^y(x, z_m) \quad (9)$$

where  $x$  is the downwind distance pointing against the average horizontal wind direction,  $y$  is the crosswind wind distance,  $z_m$  is the measurement height,  $f^y(x, z_m)$  is the crosswind integrated footprint, and  $D_y(x, y)$  is the Gaussian crosswind distribution function of the lateral dispersion. It is worth noting that the observed wind velocity at  $z_m$  was used as an input item to gain the model parameters.

For LAS flux observations, by combining the path-weighting function of LAS (Meijninger et al., 2002a) with the above point flux footprint model, we deduce,

$$f_{\text{LAS}}(x', y', z_m) = \int_{x_2}^{x_1} W(x) f(x - x', y - y', z_m) dx \quad (10)$$

where  $W(x)$  is the path-weighting function of LAS,  $x_1, x_2$  are the locations of the transmitter and receiver of LAS,  $x, y$  denote the points along the optical length of LAS, and  $x', y'$  are the coordinates upwind of each points  $(x, y)$ .

To obtain the monthly flux source area of the EC and LAS flux measurements, we determined the monthly footprint by averaging every half-hourly footprint when the sensible heat fluxes were larger than zero. Values ranging from 22:00 to 06:00 BST (Beijing standard time) were also excluded. We chose an area of 3 km  $\times$  3 km with a 30 m resolution as an approximate area of the total source area around the measurement point for EC and the central part of the LAS optical path, respectively. We then set the flux contribution of the chosen total source area at 80% for each month and 95% for every 30 min.

## Measurements of energy and water vapor fluxes in the Heihe River Basin

S. Liu et al.

Title Page

Abstract

Introduction

Conclusions

References

Tables

Figures

⏪

⏩

◀

▶

Back

Close

Full Screen / Esc

Printer-friendly Version

Interactive Discussion



## 2.2.5 Remote sensing data

The remote sensing data used in this study included the ASTER (Advanced Spaceborne Thermal Emission and Reflection radiometer) surface temperature product (2B03) and the Landsat TM5 (Thematic Mapper) images. The ASTER surface temperature product was collected on 25 March and 15 July 2008, with an overpass time of 12:30 BST (Beijing standard time). The resolution was 90 m, which was resampled to 30 m. For the Landsat TM5 image, the surface temperature on 21 April and 24 June 2009, were retrieved using the mono-window algorithm (Qin et al., 2001). The overpass time of Landsat was 12:00 BST, and the resolution was resampled from the initial 60 m to 30 m.

## 3 Results and discussion

### 3.1 Source areas of flux measurements

The source areas of the EC and LAS measurements in January, April, July and October of 2008 at YK, AR and GT (January and April of 2009 at AR) are shown in Fig. 3.

As can be seen from Fig. 3, the source areas of EC in January and April were larger than in July and October at YK, and the shape changed with wind direction in each month. However, the main contributing source area of the EC measurements in each month was within a 180 m radius of the observation point at YK, and the contribution ratio increased to a maximum approximately 30 m away from the observation point. At AR, the source area of the EC measurements distributed from southeast to northwest in each month, and the area within 400 m (east–west) and 200 m (south–north) provided the main contribution. The contribution ratio reached its maximum at about 30 m away from the EC system. At GT, the source areas of EC in each month extended from the southwest to northeast, with the main contribution area localized within 460 m (south–north) and 450 m (east–west). The source areas in April and October were

## Measurements of energy and water vapor fluxes in the Heihe River Basin

S. Liu et al.

Title Page

Abstract

Introduction

Conclusions

References

Tables

Figures



Back

Close

Full Screen / Esc

Printer-friendly Version

Interactive Discussion



a little larger than January and July, and the maximum contribution ratio was about 50 m away from the EC system. The source areas of the LAS measurements at AR extended from the northeast to the southwest, with the main contribution source area about 700 m wide and 2000 m long.

5 The source area of the EC measurements at each site extended along the prevailing wind direction. The source area of the LAS measurements was along its optical path and was typically distributed on both sides of the optical path. The source area's exact shape primarily depended on the measurement height, the wind direction and the stability of the atmosphere. At YK, for example, the prevailing wind directions were north and northeast in January. Thus, the main contribution source areas of the EC measurements extended in the same directions, and the dominant wind directions were north and west in July. Therefore, the contributions of the two directions were higher than the other directions. Similar results were observed at the other two sites. At YK, the underlying surface of the EC's source areas consisted mainly of bare soil in 10 January, April and October, and maize interplanted with spring wheat in July. The underlying surface within the source areas of the EC and LAS measurements around AR was alpine meadow. The EC's source areas at GT were covered with forest (Qinghai spruce) (Fig. 2).

## 3.2 Seasonal variations of energy and water vapor fluxes

### 3.2.1 Energy balance closure of EC

20 To show the energy balance closure at the three sites, the turbulent energy fluxes (the sum of sensible heat flux  $H$  and latent heat flux  $LE$ ) were plotted against the available energy (net radiation  $R_n$  minus soil surface heat flux  $G_0$ ) in Fig. 4, using the half-hourly data obtained during the period from January to December at YK and GT in 2008 and 25 2009 and the period from June to December in 2008 and January to December in 2009 at AR. The soil surface heat flux ( $G_0$ ) was obtained at each site using Eq. (8).

## Measurements of energy and water vapor fluxes in the Heihe River Basin

S. Liu et al.

Title Page

Abstract

Introduction

Conclusions

References

Tables

Figures



Back

Close

Full Screen / Esc

Printer-friendly Version

Interactive Discussion





the range of 79% to 89% in this study, so it seems that there were other reasons for the imbalance. According to recent studies (Mauder et al., 2007b; Foken, 2008), low-frequency eddies and turbulent organized structures (TOS) that cannot be measured by the EC maybe one of the main causes of the energy imbalance.

### 3.2.2 Seasonal variation of energy balance components

To clearly describe the partitioning of energy balance components in different seasons, the diurnal patterns of the half-hourly averages of  $R_n$ , LE,  $H$  (sensible heat flux measured by LAS is denoted by  $H_{LAS}$ ), and  $G_0$  in January, April, July and October for 2008 (January and April in 2009 at AR) are plotted in Fig. 5. Table 2 summarizes the ratios of LE,  $H$ , and  $G_0$  to  $R_n$ , on the monthly average basis, and it describes the monthly ET at each site.

Figure 5 and Table 2 show the change in energy partitioning at each site with the variation of season (from  $H$  to LE dominated during January to July, and from LE back to  $H$  dominated during July to October). The soil surface heat flux accounted for a small proportion especially in GT, where the underlying surface was forest with moss cover. The partitioning of net radiation into sensible and latent heat flux was strongly influenced by changes in vegetation characteristics. Specifically, all plants were dormant in January and April, and the surrounding surface in the EC source area was composed of bare soil, withered grassland, and dormant forest at YK, AR and GT, respectively (see Sect. 3.1). Therefore, the sensible heat flux was the main energy consumption in January ( $H/R_n$  at YK: 51%; AR: 49%; GT: 51%), while the proportions of LE and  $G_0$  to  $R_n$  were small. The dominant component of the energy budget was also  $H$  in April ( $H/R_n$  at YK: 36%; AR: 47%; GT: 55%).

In July, the underlying surface of the EC source areas were maize interplanted with spring wheat, growing grassland and Qinghai spruce at YK, AR and GT, respectively. Thus, the LE increased to account for 74%, 58% and 41% of  $R_n$  at YK, AR and GT, respectively. The soil surface heat flux  $G_0$  accounted for a relatively small proportion at each site (about 12% at YK, 13% at AR and 0.04% at GT). One special phenomena

## Measurements of energy and water vapor fluxes in the Heihe River Basin

S. Liu et al.

Title Page

Abstract

Introduction

Conclusions

References

Tables

Figures

⏪

⏩

◀

▶

Back

Close

Full Screen / Esc

Printer-friendly Version

Interactive Discussion



## Measurements of energy and water vapor fluxes in the Heihe River Basin

S. Liu et al.

Title Page

Abstract

Introduction

Conclusions

References

Tables

Figures

⏪

⏩

◀

▶

Back

Close

Full Screen / Esc

Printer-friendly Version

Interactive Discussion



which called “oasis effect” should be noted for YK in July: (1) the average diurnal course of LE was the main component, and the monthly ET also reached the peak of 160.70 mm (Fig. 5c and Table 2); and (2)  $H$  was very small, and even negative in the afternoon when the heat transferred downward and a temperature inversion occurred.

This phenomenon is consistent with the results obtained in the Heihe River Basin by Wang et al. (1999). YK was located in the center of an oasis surrounded by Gobi (the nearest extent is about 7 km from the site, see Fig. 2a), and the “oasis effect” was distinctly observed on clear days in summer.

In October, the underlying surfaces in the EC source areas appeared to be almost the same as in April. LE was also small at AR and GT, and  $H/R_n$  was 43% at AR and 48% at GT. Although crops had been harvested at YK, because of the application of autumn irrigation (post-harvest irrigation), LE was still the main term in the energy budget, accounting for 36% of  $R_n$ . These results indicate that the surface energy budget at each site was mainly determined by local meteorological events, vegetative conditions and soil water content in the source area of the flux measurements. For example, the LE at YK was much higher than at the other two sites during the growing season because of irrigation.

The sensible heat flux measured by LAS ( $H_{LAS}$ ) also exhibited significant seasonal variation at AR. The underlying surface of the LAS source area was withered grassland in January, April and October and growing grass in July (see Sect. 3.1). The ratios of  $H_{LAS}$  to  $R_n$  were 61%, 51%, 15%, and 41% in January, April, July and October, respectively (Table 2). Although the tendency and magnitude of sensible heat fluxes measured by LAS and EC were similar, there was still a difference between LAS and EC.

### 3.2.3 Seasonal variations of evapotranspiration

In this section, we focus on analyzing the seasonal variations of ET from the EC and LAS at YK, AR and GT from January (March at AR) 2008 to December 2009 (March to October in 2008 and January to June in 2009 for LAS data).



$C_T^2 (Z_{LAS}-d)^{2/3} / T_*^2$  were plotted against  $(Z_{LAS}-d)/L_{MO}$  in Fig.7 for the entire selected data set; and values of  $T_*$  and  $L_{MO}$  were taken from the EC measurements together with the scaling curves found by De Bruin et al. (1993), Andreas (1988) and Thiermann and Grassl (1992). Figure 7 shows that these points follow the shape of the universal functions. This result also implies that the MOST relationship (Eq. 3) was fully applicable at AR.

The data for the period from 11 March to 31 October 2008, and from 1 January to 30 June 2009, were used for this analysis, and the sensible heat fluxes measured by EC ( $H_{ec}$ ) and LAS ( $H_{LAS}$ ) were compared. The results are shown in Fig. 8 only when  $H_{ec}$  and  $H_{LAS}$  larger than  $50 \text{ W m}^{-2}$  were used. Figure 8 shows that  $H_{LAS}$  was consistent with  $H_{ec}$  ( $R^2=0.65$ , for data points  $n=3575$ ), but  $H_{LAS}$  was generally larger than  $H_{ec}$ .

The reasons for the differences between the sensible heat fluxes of LAS and EC have been investigated by many researchers. Schüttemeyer et al. (2006) found that the heterogeneity of the underlying surface caused the differences between the LAS and EC measurements in a mixed vegetation area. Ezzahar et al. (2007) considered that the differences between the two measurements could be explained by the difference in terms of the source areas of the LAS and EC and the closure failure of the energy balance of the EC. The EBR at AR was 0.89/0.85 in 2008/2009 (see Sect. 3.2.1). To evaluate the influence of the energy imbalance on the difference between  $H_{ec}$  and  $H_{LAS}$ , the EBR of EC per 30 min versus the ratio of  $H_{ec}$  and  $H_{LAS}$  ( $H_{ec}/H_{LAS}$ ) at AR were plotted in Fig. 9. As can be seen from Fig. 9, the ratio generally increased with the increase of the EBR. That is to say, when the EBR increased, the values of  $H_{ec}$  were closer to  $H_{LAS}$ . When the EBR was small, the values of  $H_{ec}$  were obviously smaller than  $H_{LAS}$ , especially when the EBR was less than 0.75. However, in the EBR range between 0.75 and 1, most of the values ( $H_{ec}/H_{LAS}$ ) concentrated around the line of  $H_{ec}/H_{LAS}=1$ . When their EBRs were larger than 0.75, these points were replotted in Fig. 10. As can be seen from Fig. 10, the  $H_{ec}$  and  $H_{LAS}$  were much closer to each other, with only a 6% difference ( $R^2=0.67$ ,  $n=1202$ ). Therefore, one can conclude that

**Measurements of energy and water vapor fluxes in the Heihe River Basin**

S. Liu et al.

Title Page

Abstract

Introduction

Conclusions

References

Tables

Figures

◀

▶

◀

▶

Back

Close

Full Screen / Esc

Printer-friendly Version

Interactive Discussion



the energy imbalance of EC was one of main causes of the difference between  $H_{ec}$  and  $H_{LAS}$  at AR.

From the above analysis, we found that the energy imbalance of EC was one of the reasons for the difference between the LAS and EC measurements at AR; however, it was not the sole reason. Hoedjes et al. (2007) found that radiative surface temperatures obtained from thermal infrared satellite imagery can provide a good indication of the degree of heterogeneity within the experimental area and can be used to identify the differences between LAS and EC measurements of sensible heat fluxes. In this study, the surface temperatures ( $T_s$ ) from four satellite images were used to further analyze the reasons for the difference between  $H_{ec}$  and  $H_{LAS}$ , namely, two ASTER images (25 March and 15 July 2008) and two TM images (21 April and 24 June 2009). The processing steps of these images are shown in Sect. 2.2.5. The standard deviation of surface temperatures in the non-overlapping source area ( $Std\_T_s$ ) at the time of satellite overpass was chosen to reflect the heterogeneity of the underlying surface, and the standard deviation of surface temperatures in the non-overlapping source area

was calculated by  $Std\_T_s = \sqrt{\left(\frac{1}{n-1} \sum_{i=1}^n (T_{si} - \bar{T}_s)^2\right)}$ , where  $T_{si}$  and  $\bar{T}_s$  are the surface temperature values per pixel and the average value within the non-overlapping source area, respectively, and  $n$  is the number of pixels. The average normalized relative weights of EC and LAS in the overlapping source area ( $Ave\_RW$ ) was chosen to quantify the differences between the source areas of the LAS and EC. The average normalized relative weights of the EC and LAS were estimated by  $Ave\_RW = \frac{1}{2} \left( \sum_{i=1}^m FP_{LASi} + \sum_{i=1}^m FP_{eci} \right)$ , where  $FP_{LASi}$  and  $FP_{eci}$  are the normalized footprint of EC and LAS per grid within the overlapped source area, respectively, and  $m$  is the number of grids within the overlapped source area. Generally speaking, when the source area of LAS was coincident with EC,  $Ave\_RW$  was equal to 1. That is to say, the  $Ave\_RW$  value was much closer to 1, and the degree of overlap between the source areas of the LAS and EC measurements was much larger. Table 3 shows the relationships among the differences of the

## Measurements of energy and water vapor fluxes in the Heihe River Basin

S. Liu et al.

[Title Page](#)[Abstract](#)[Introduction](#)[Conclusions](#)[References](#)[Tables](#)[Figures](#)[⏪](#)[⏩](#)[◀](#)[▶](#)[Back](#)[Close](#)[Full Screen / Esc](#)[Printer-friendly Version](#)[Interactive Discussion](#)

EC and LAS measurements ( $H_{ec}/H_{LAS}$ ), the energy closure ratio of EC (EBR), the degree of overlap between the source areas of the LAS and EC measurements (Ave\_RW), and the heterogeneity of the underlying surface (Std\_ $T_s$ ) at the time of satellite overpass. The greatest difference between  $H_{ec}$  and  $H_{LAS}$  ( $H_{ec}/H_{LAS}=1.17$ ) appeared on 25 March 2008, with the smallest EBR (0.81), a tiny Ave\_RW (0.001) and the largest Std\_ $T_s$  (2.16 K). The smallest difference between  $H_{ec}$  and  $H_{LAS}$  ( $H_{ec}/H_{LAS}=0.98$ ) appeared on 24 June 2009, with the corresponding smallest Std\_ $T_s$  (0.93 K), the largest Ave\_RW (0.51), and a higher EBR (0.89) during the four days. This result indicates that the differences between the EC and LAS measurements ( $H_{ec}/H_{LAS}$ ) can be explained by the energy closure ratio of EC (EBR), the degree of overlap between the source areas of the LAS and EC measurements (Ave\_RW), and the heterogeneity of the underlying surface (Std\_ $T_s$ ). All the three factors have an effect on the differences between  $H_{ec}$  and  $H_{LAS}$ , and their effects were coupled with each other. Taking 25 March 2008, and 21 April and 24 June 2009 as an example, similar EBR values were observed on the three days; the differences between  $H_{ec}$  and  $H_{LAS}$  increased with the decreasing Ave\_RW and increasing Std\_ $T_s$ . Comparing 24 June 2009 and 25 July 2008, when the Ave\_RW on these two days was very close to each other, the difference of EBR and Std\_ $T_s$  led to the discrepancy of  $H_{ec}/H_{LAS}$ . Generally speaking, all the three factors can cause the differences between  $H_{ec}$  and  $H_{LAS}$ .

From these analyses, we conclude that the differences between sensible heat fluxes derived from LAS and EC at AR were caused by the energy imbalance of EC, the heterogeneity of the underlying surfaces, and the difference between the source areas of the EC and LAS measurements.

# HESSD

7, 8741–8780, 2010

## Measurements of energy and water vapor fluxes in the Heihe River Basin

S. Liu et al.

Title Page

Abstract

Introduction

Conclusions

References

Tables

Figures

⏪

⏩

◀

▶

Back

Close

Full Screen / Esc

Printer-friendly Version

Interactive Discussion



## 4 Conclusions

In this study, we analyzed the seasonal variations of energy and water vapor fluxes at YK (irrigated cropland), AR (alpine meadow), and GT (spruce forest) based on measurements made by EC and LAS in the Heihe River Basin, China. We also determined the source areas of EC and LAS for each site and discussed the factors causing the differences between sensible heat fluxes measured by EC and LAS at AR.

The source areas of EC differed significantly at the three sites, and the main contributing areas were within a radius of 250 m. The main contribution area for LAS extended along a path about 2000 m long and 700 m wide at AR. The surface characteristics in the source area changed with time at the three sites which had a major influence on the surface energy budget.

The sensible heat flux was the main term of the heat budget at the three sites during the dormant season. During the growing season, however, the latent heat flux was the main term at YK and AR, and an obvious “oasis effect” was observed at YK. The ET at the three sites exhibited a “single peak” pattern, and the monthly ET reached its peak in July at YK and June at GT in both 2008 and 2009, while it reached its peak in August at AR in 2008 and in June in 2009. The annual ET at YK in the irrigated cropland was much larger than that of the other two sites.

We compared the differences between sensible heat fluxes derived from LAS and EC at AR in grassland. The results showed that the sensible heat flux from LAS were, on average, larger than EC, especially when the EBR was smaller than 0.75. The thermal infrared satellite images in combination with a footprint model were used to indicate of the heterogeneity within the non-overlapping source area between LAS and EC, and the overlapping ratio was used to reflect the difference between the source areas of LAS and EC. The results of this study show that the difference between sensible heat fluxes derived from LAS and EC at AR can be explained by the energy imbalance of EC, the heterogeneity of the underlying surfaces, and the differences between the source areas of the EC and LAS measurements.

## Measurements of energy and water vapor fluxes in the Heihe River Basin

S. Liu et al.

Title Page

Abstract

Introduction

Conclusions

References

Tables

Figures



Back

Close

Full Screen / Esc

Printer-friendly Version

Interactive Discussion



*Acknowledgements.* The data used in the paper are obtained from the Watershed Allied Telemetry Experimental Research, which is jointly supported by the Special Research Foundation of the Public Benefit Industry (GYHY200706046), National Natural Science Foundation of China (40971194 and 40875006), the Chinese state key basic research project (2007CB714400) and the Chinese academy of sciences action plan for west development program (KZCX2-XB2-09). The ASTER data used in the paper are provided by Shunlin Liang.

## References

- Andreas, E. L.: Estimating  $C_n^2$  over snow and sea ice from meteorological data, *J. Opt. Soc. Am.*, 5, 481–495, 1988.
- Aubinet, M., Grelle, A., Ibrom, A., Rannik, U., Moncrieff, J., Foken, T., Kowalski, A. S., Martin, P. H., Berbigier, P., Bernhofer, C., Clement, R., Elbers, J., Granier, A., Grünwald, T., Morgenstern, K., Pilegaard, K., Rebmann, C., Snijders, W., Valentini, R., and Vesala, T.: Estimates of the annual net carbon and water exchange of European forests: the EUROFLUX methodology, *Adv. Ecol. Res.*, 30, 113–174, 2000.
- Baldocchi, D. D., Vogel, C. A., and Hall, B.: Seasonal variation of carbon dioxide exchange rates above and below a boreal jack pine forest, *Agr. Forest Meteorol.*, 83, 147–170, 1997.
- Blanken, P. D., Black, T. A., Neumann, H. H., Hartog, C. D., Yang, P. C., Nescic, Z., Staebler, R., Chen, W., and Novak, M. D.: Turbulence flux measurements above and below the overstory of a boreal aspen forest, *Bound.-Lay. Meteorol.*, 89, 109–140, 1998.
- Businger, J. A., Wyngaard, J. C., Izumi, Y., and Bradley, E. F.: Flux profile relationships in the atmospheric surface layer, *J. Atmos. Sci.*, 28, 181–189, 1971.
- Cava, D., Contini, D., Donato, A., and Martano, P.: Analysis of short-term closure of the surface energy balance above short vegetation, *Agr. Forest Meteorol.*, 148, 82–93, 2008.
- De Bruin, H. A. R., Kohsiek, W., and Hurk, V.: A verification of some methods to determine the fluxes of momentum, sensible heat and water vapor using standard deviation and structure parameter of scalar meteorological quantities, *Bound.-Lay. Meteorol.*, 63, 231–257, 1993.
- Ezzahar, J., Chehbouni, A., Hoedjes, J. C. B., Er-Raki, S., Chehbouni, A., Boulet, G., Bonfond, J. M., and De Bruin, H. A. R.: The use of the scintillation technique for monitoring seasonal water consumption of olive orchards in a semi-arid region, *Agr. Water Manage.*, 89, 173–184, 2007.

## Measurements of energy and water vapor fluxes in the Heihe River Basin

S. Liu et al.

Title Page

Abstract

Introduction

Conclusions

References

Tables

Figures

⏪

⏩

◀

▶

Back

Close

Full Screen / Esc

Printer-friendly Version

Interactive Discussion





## Measurements of energy and water vapor fluxes in the Heihe River Basin

S. Liu et al.

[Title Page](#)
[Abstract](#)
[Introduction](#)
[Conclusions](#)
[References](#)
[Tables](#)
[Figures](#)




[Back](#)
[Close](#)
[Full Screen / Esc](#)
[Printer-friendly Version](#)
[Interactive Discussion](#)

- Jacobs, A. F. G., Heusinkveld, B. G., and Holtslag, A. A. M.: Towards closing the surface energy budget of a mid-latitude Grassland, *Bound.-Lay. Meteorol.*, 126, 125–136, 2008.
- Kanda, M., Inagaki, A., Letzel, M. O., Raasch, S., and Watanabe, T.: LES study of the energy imbalance problem with eddy covariance fluxes, *Bound.-Lay. Meteorol.*, 110, 381–404, 2004.
- Kormann, R. and Meixner, F. X.: An analytic footprint model for neutral stratification, *Bound.-Lay. Meteorol.*, 99, 207–224, 2001.
- Li, X., Li, X. W., Li, Z. Y., Ma, M. G., Wang, J., Xiao, Q., Liu, Q., Che, T., Chen, E. X., Yan, G. J., Hu, Z. Y., Zhang, L. X., Chu, R. Z., Su, P. X., Liu, Q. H., Liu, S. M., Wang, J. D., Niu, Z., Chen, Y., Jin, R., Wang, W. Z., Ran, Y. H., Xin, X. Z., and Ren, H. Z.: Watershed allied telemetry experimental research, *J. Geophys. Res.-Atmos.*, 114, D22103, doi:10.1029/2008JD011590, 2009.
- Mauder, M., Liebenthal, C., Göckede, M., Leps, J. P., Beyrich, F., and Foken, T.: Processing and quality control of flux data during LITFASS-2003, *Bound.-Lay. Meteorol.*, 121, 67–88, 2006.
- Mauder, M., Oncley, S. P., Vogt, R., Weidinger, T., Ribeiro, L., Bernhofer, C., Foken, T., Kohsiek, W., De Bruin, H. A. R., and Liu, H. P.: The energy balance experiment EBEX-2000, Part II: Intercomparison of eddy-covariance sensors and post-field data processing methods, *Bound.-Lay. Meteorol.*, 123, 29–54, 2007a.
- Mauder, M., Desjardins, R. L., and MacPherson, I.: Scale analysis of airborne flux measurements over heterogeneous terrain in a boreal ecosystem, *J. Geophys. Res.*, 112, D13112, doi:10.1029/2006JD008133, 2007b.
- McAneney, K. J., Green, A. E., and Astill, M. S.: Large aperture scintillometry: the homogeneous case, *Agr. Forest Meteorol.*, 76, 149–162, 1995.
- Meijninger, W. M. L., Hartogensis, O. K., Kohsiek, W., Hoedjes, J. C. B., Zuurbier, R. M., and De Bruin, H. A. R.: Determination of the area-averaged sensible heat flux with a large aperture scintillometer over a heterogeneous surface-Flevoland field experiment, *Bound.-Lay. Meteorol.*, 105, 37–62, 2002a.
- Meijninger, W. M. L., Green, A. E., Hartogensis, O. K., Kohsiek, W., Hoedjes, C. B., Zuurbier, R. M., and De Bruin, H. A. R.: Determination of area-averaged water vapour fluxes with large aperture and radio wave scintillometers over a heterogeneous surface-Flevoland field experiment, *Bound.-Lay. Meteorol.*, 105, 63–83, 2002b.
- Meyers, T. P. and Hollinger, S. E.: An assessment of storage terms in the surface energy balance of maize and soybean, *Agr. Forest Meteorol.*, 125, 105–115, 2004.

## Measurements of energy and water vapor fluxes in the Heihe River Basin

S. Liu et al.

Title Page

Abstract

Introduction

Conclusions

References

Tables

Figures

⏪

⏩

◀

▶

Back

Close

Full Screen / Esc

Printer-friendly Version

Interactive Discussion

- Michiles, A. A. S. and Gielow, R.: Above-ground thermal energy storage rates, trunk heat fluxes and surface energy balance in a Central Amazonian rainforest, *Agr. Forest Meteorol.*, 148, 917–930, 2008.
- Milly, P. C. D. and Dunne, K. A.: Trends in evaporation and surface cooling in the Mississippi River Basin, *Geophys. Res. Lett.*, 28, 1219–1222, 2001.
- Moene, A. F., Beyrich, F., and Hartogensis, O. K.: Developments in scintillometry, *B. Am. Meteorol. Soc.*, 90, 694–698, 2009.
- Ochs, G. R. and Wilson, J. J.: A second-generation large aperture scintillometer, NOAA Tech. Memor. ERL ETL-232, NOAA Environmental Research Laboratories, Boulder, CO, USA, 24 pp., 1993.
- Oncley, S. P., Foken, T., Vogt, R., Kohsiek, W., De Bruin, H. A. R., Bernhofer, C., Christen, A., Gorsel, E. V., Grantz, D., Feigenwinter, C., Lehner, I., Liebenthal, C., Liu, H. P., Mauder, M., Pitacco, A., Ribeiro, L., and Weidinger, T.: The energy balance experiment EBEX-2000, Part I: overview and energy balance, *Bound.-Lay. Meteorol.*, 123, 1–28, 2007.
- Paulson, C. A.: The mathematical representation of wind speed and temperature profiles in the unstable atmospheric surface layer, *J. Appl. Meteorol.*, 9, 857–861, 1970.
- Qin, Z., Zhang, M., Karnieli, A., and Berliner, P.: Mono-window algorithm for retrieving land surface temperature from Landsat TM6 data, *Acta Geogr. Sinica*, 4, 456–466, 2001.
- Rosenberg, N. J., Blad, B. L., and Verma, S. B.: *Microclimate – the Biological Environment of Plants*, 2nd edition, John Wiley and Sons, New York, 495 pp., 1983.
- Schmid, H. P.: Footprint modeling for vegetation atmosphere exchange studies: a review and perspective, *Agr. Forest Meteorol.*, 113, 159–183, 2002.
- Schüttemeyer, D., Moene, A. F., Holtslag, A. A. M., De Bruin, H. A. R., and De Giesen, N. A.: Surface fluxes and characteristics of drying semi-arid terrain in West Africa, *Bound.-Lay. Meteorol.*, 118, 583–612, 2006.
- Steinfeld, G., Letzel, M. O., Raasch, S., Kanda, M., and Inagaki, A.: Spatial representativeness of single tower measurements and the imbalance problem with eddy-covariance fluxes: results of a large-eddy simulation study, *Bound.-Lay. Meteorol.*, 123, 77–98, 2007.
- Suyker, A. E. and Verma, S. B.: Interannual water vapor and energy exchange in an irrigated maize-based agroecosystem, *Agr. Forest Meteorol.*, 148, 417–427, 2008.
- Thiermann, V. and Grassl, H.: The measurement of turbulent surface layer fluxes by use of bichromatic scintillation, *Bound.-Lay. Meteorol.*, 58, 367–389, 1992.

## Measurements of energy and water vapor fluxes in the Heihe River Basin

S. Liu et al.

Title Page

Abstract

Introduction

Conclusions

References

Tables

Figures

⏪

⏩

◀

▶

Back

Close

Full Screen / Esc

Printer-friendly Version

Interactive Discussion



- Twine, T. E., Kustas, W. P., Norman, J. M., Cook, D. R., Houser, P. R., Meyers, T. P., Prueger, J. H., Starks, P. J., and Wesely, M. L.: Correcting eddy-covariance flux underestimates over grassland, *Agr. Forest Meteorol.*, 103, 279–300, 2000.
- Von Randow, C., Kruijt, B., Holtslag, A. A. M., and De Oliveira, A. B. L.: Exploring eddy-covariance and large-aperture scintillometer measurements in an Amazonian rain forest, *Agr. Forest Meteorol.*, 148, 680–690, 2008.
- Wang, T., Ochs, G., and Clifford, S.: Saturation-Resistant optical scintillometer to measure  $Cn_2$ , *J. Opt. Soc. Am.*, 68, 334–338, 1978.
- Wang, J. M.: Land surface process experiments and interaction study in China – from HEIFE to IMGRASS and GAME Tibet/TIPEX, *Plateau Meteorol.*, 18, 280–294, 1999.
- Wang, W. H., Liang, S. L., and Meyers, T.: Validating MODIS land surface temperature products using long-term nighttime ground measurements, *Remote Sens. Environ.*, 112, 623–635, 2008.
- Webb, E. K.: Profile relationships: the log-linear range and extension to strong stability, *Q. J. Roy. Meteor. Soc.*, 96, 67–90, 1970.
- Wesely, M. L.: The combined effect of temperature and humidity fluctuations on refractive index, *J. Appl. Meteorol.*, 15, 43–49, 1976.
- Wever, L. A., Flanagan, L. B., and Carlson, P. J.: Seasonal and interannual variation in evapotranspiration, energy balance and surface conductance in a northern temperate grassland, *Agr. Forest Meteorol.*, 112, 31–49, 2002.
- Wilson, K. B. and Baldocchi, D. D.: Seasonal and interannual variability of energy fluxes over a broadleaved temperate deciduous forest in North America, *Agr. Forest Meteorol.*, 100, 1–18, 2000.
- Wilson, K. B., Goldstein, A., Falg, E., Aubinet, M., Baldocchi, D., Berbigier, P., Bernhofer, C., Ceulemans, R., Dolman, H., Field, C., Grelle, A., Ibrom, A., Law, B. E., Kowalski, A., Meyers, T., Moncrieff, J., Monson, R., Oechel, W., Tenhunen, J., Valentini, R., and Verma, S.: Energy balance closure at FLUXNET sites, *Agr. Forest Meteorol.*, 113, 223–243, 2002.
- Yang, K., Koike, T., and Yang, D.: Surface flux parameterization in the Tibetan Plateau, *Bound.-Lay. Meteorol.*, 116, 245–262, 2003.
- Yang, K. and Wang, J. M.: A temperature prediction-correction method for estimating surface soil heat flux from soil temperature and moisture data, *Sci. China Ser. D*, 51, 721–729, 2008.

## Measurements of energy and water vapor fluxes in the Heihe River Basin

S. Liu et al.

**Table 1.** Description of the instruments incorporated in the EC, LAS and AWS at each site.

Instrument	Variable	Sensors				Height/path length (m)	
		YK	AR	GT	YK	AR	GT
EC	Sensible heat flux and Latent heat flux	Li7500 and CSAT3, Li-cor and Campbell	Li7500 and KH <sub>2</sub> O Li-cor and Campbell (11 Mar 2008~2 Apr 2008) Li7500 and CSAT3, Li-cor and Campbell (10 Jun 2008~31 Dec 2009)	Li7500 and CSAT3, Li-cor and Campbell	2.81	3.15	20.25
LAS	Sensible heat flux		BLS450, Scintec (2008.03.11~2008.10.31, 2009.01.01~2009.06.30)			9.5/2390	
AWS	Air temperature /humidity	HMP45C, Vaisala	HMP45C, Vaisala	HMP45C, Vaisala	3, 10	2, 10	2, 10, 24
	Wind speed	010C-1, Metone	014A, Metone	014A/034B, Metone	3, 10	2, 10	2, 10, 24
	Wind direction	020C-1, Metone	034B, Metone	034B, Metone	10	10	24
	Short wave radiation	CM3, Kipp and Zonen	PSP, Eppley	CM3, Kipp and Zonen	4	1.5	19.75
	Long wave radiation	CG3, Kipp and Zonen	PIP, Eppley	CG3, Kipp and Zonen	4	1.5	19.75
	Soil heat flux	HFP01, Hukeflux 109, Campbell	HFT3, Campbell	HFP01, Hukeflux 107, Campbell	0.05, 0.15	0.05, 0.15	0.05, 0.15
	Soil temperature				0.1, 0.2, 0.4, 0.8, 1.2, 1.6	0.1, 0.2, 0.4, 0.8, 1.2, 1.6	0.05, 0.1, 0.2, 0.4, 0.8, 1.2
	Soil moisture	CS616, Campbell	CS616, Campbell	CS616, Campbell	0.1, 0.2, 0.4, 0.8, 1.2, 1.6	0.1, 0.2, 0.4, 0.8, 1.2, 1.6	0.05, 0.1, 0.2, 0.4, 0.8, 1.2
	Air pressure	CS100, Campbell	CS105, Vaisala	CS105, Vaisala	–	–	–
	Precipitation	52202 R. M.Young	TE525, Campbell	52202 R. M. Young	–	–	–
Landscape		YK: Cropland (maize, wheat), AR: Alpine meadow, GT: Forest (Qinghai spruce)					
Vegetation Height		YK: the maximum height of 1 m for sprint wheat, and 1.8 m for maize AR: the maximum height of 0.2–0.3 m for grass GT: forest canopy height of 18–20 m					



Title Page

Abstract Introduction

Conclusions References

Tables Figures

◀ ▶

◀ ▶

Back Close

Full Screen / Esc

Printer-friendly Version

Interactive Discussion

## Measurements of energy and water vapor fluxes in the Heihe River Basin

S. Liu et al.

**Table 2.** Ratios of monthly LE,  $H$ ,  $G_0$  to  $R_n$ , and ET during different seasons at the three sites in 2008 (January and April 2009 at AR; values in the bracket are  $H_{LAS}/R_n$ ).

Sites	Date	LE/ $R_n$	$H/R_n$	$G_0/R_n$	ET (mm)
YK	Jan	0.13	0.51	0.28	2.92
	Apr	0.32	0.36	0.10	52.02
	Jul	0.74	0.002	0.12	160.70
	Oct	0.36	0.35	0.16	46.02
AR	Jan	0.12	0.49 (0.61)	0.18	5.45
	Apr	0.39	0.47 (0.51)	0.19	32.36
	Jul	0.58	0.13 (0.15)	0.13	116.13
	Oct	0.26	0.43 (0.41)	0.09	30.39
GT	Jan	0.06	0.51	0.03	6.98
	Apr	0.11	0.55	0.02	25.83
	Jul	0.41	0.34	0.04	68.95
	Oct	0.14	0.48	0.02	23.70

Title Page

Abstract

Introduction

Conclusions

References

Tables

Figures

⏪

⏩

◀

▶

Back

Close

Full Screen / Esc

Printer-friendly Version

Interactive Discussion



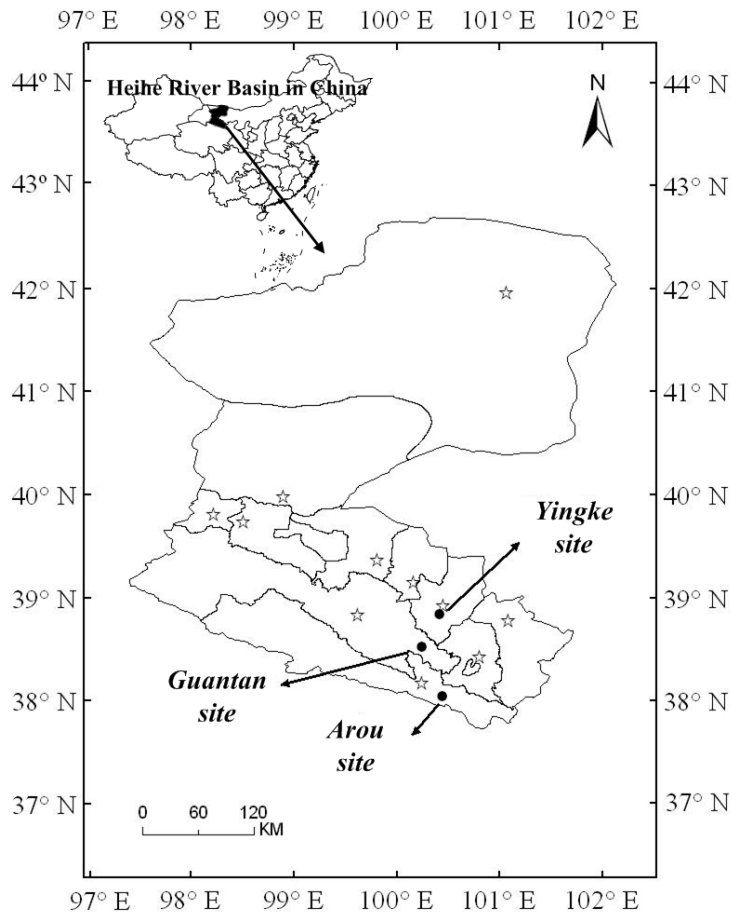


**Fig. 1.** Locations of observation sites (star symbol represents the city in the Heihe River Basin).

## Measurements of energy and water vapor fluxes in the Heihe River Basin

S. Liu et al.

Title Page	
Abstract	Introduction
Conclusions	References
Tables	Figures
◀	▶
◀	▶
Back	Close
Full Screen / Esc	
Printer-friendly Version	
Interactive Discussion	

## Measurements of energy and water vapor fluxes in the Heihe River Basin

S. Liu et al.

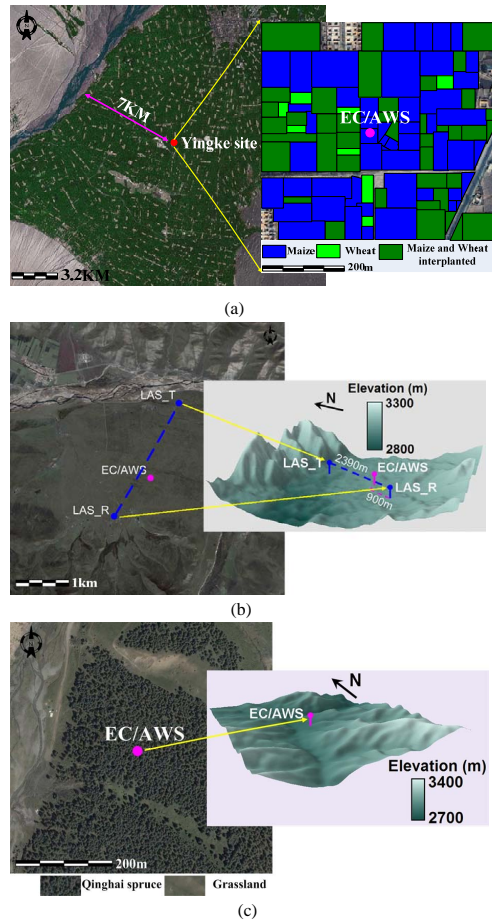


**Fig. 2.** Overview of the observation sites: **(a)** YK; **(b)** AR; **(c)** GT. The (a) and (c) images were created using Google Earth (version 5.0), 2 February 2009. (b) was a quickbird image, August 2009. A digital elevation model was also plotted in (b) and (c).

[Title Page](#)
[Abstract](#)
[Introduction](#)
[Conclusions](#)
[References](#)
[Tables](#)
[Figures](#)
[⏪](#)
[⏩](#)
[◀](#)
[▶](#)
[Back](#)
[Close](#)
[Full Screen / Esc](#)
[Printer-friendly Version](#)
[Interactive Discussion](#)

## Measurements of energy and water vapor fluxes in the Heihe River Basin

S. Liu et al.

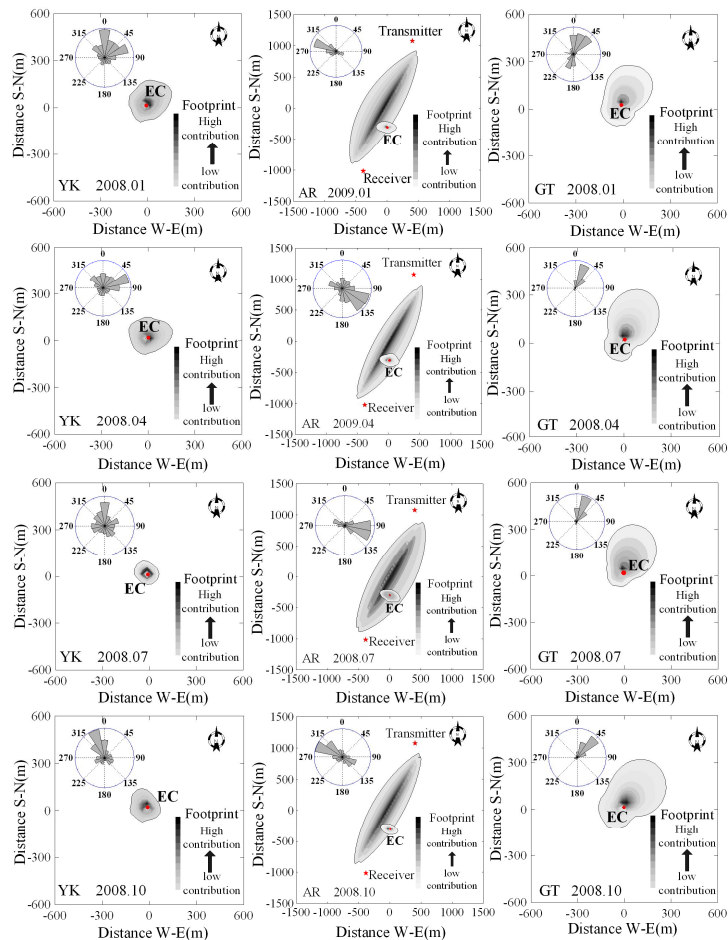


**Fig. 3.** Source areas of the LAS and EC measurements at the different sites (source area of 80% contribution to the measured fluxes).

Title Page

Abstract

Introduction

Conclusions

References

Tables

Figures

⏪

⏩

◀

▶

Back

Close

Full Screen / Esc

Printer-friendly Version

Interactive Discussion

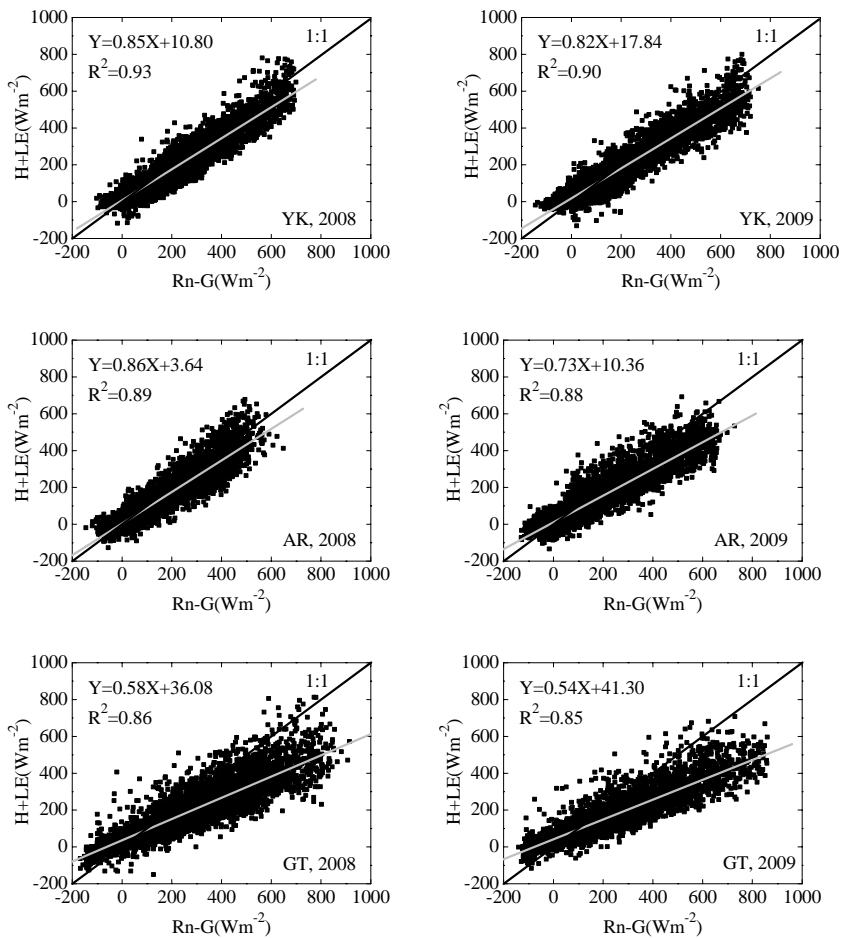


**Fig. 4.** Relationship between the available energy and the sum of the turbulent energy fluxes based on 30-min EC data at YK, AR and GT in 2008 and 2009.

## Measurements of energy and water vapor fluxes in the Heihe River Basin

S. Liu et al.

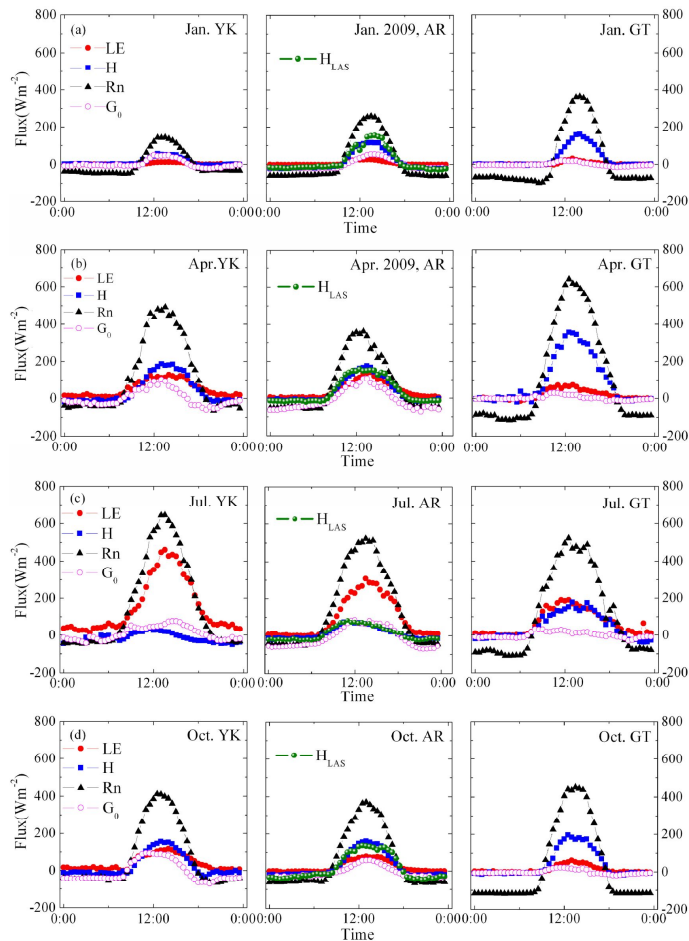


**Fig. 5.** Seasonal variations in averaged diurnal course of energy fluxes over different surfaces in 2008 (January and April 2009 at AR) (Beijing standard time, BST).

Title Page

Abstract Introduction

Conclusions References

Tables Figures

⏪ ⏩

◀ ▶

Back Close

Full Screen / Esc

Printer-friendly Version

Interactive Discussion



## Measurements of energy and water vapor fluxes in the Heihe River Basin

S. Liu et al.

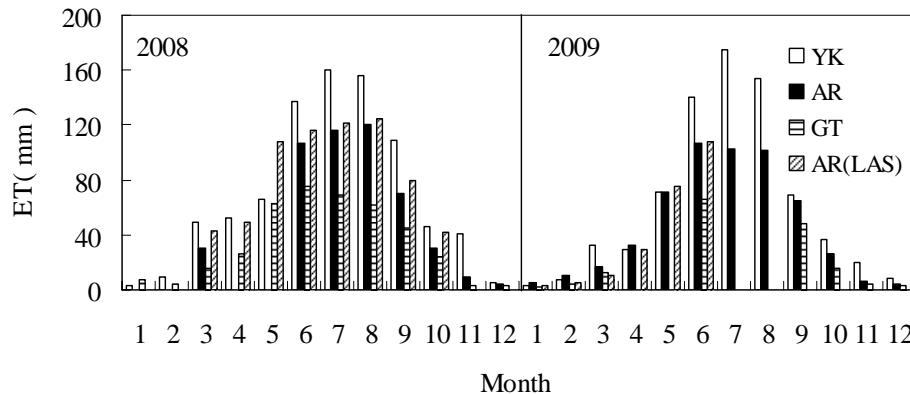


**Fig. 6.** Monthly variations of ET from EC and LAS data taken from different surfaces in 2008 and 2009.

Title Page

Abstract Introduction

Conclusions References

Tables Figures

⏪ ⏩

◀ ▶

Back Close

Full Screen / Esc

Printer-friendly Version

Interactive Discussion

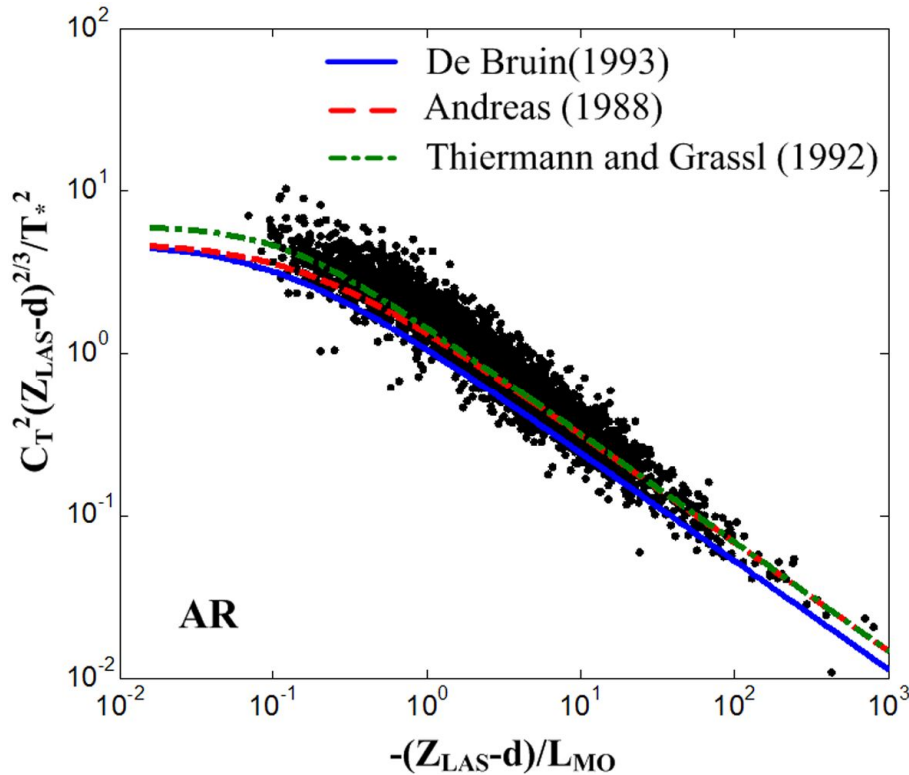


**Fig. 7.** Observed values of  $C_T^2 (Z_{LAS}-d)^{2/3} / T_*^2$  were plotted against  $(Z_{LAS}-d) / L_{MO}$  under unstable conditions for the entire dataset (11 March–31 October 2008, and 1 January–30 June 2009, 30 min,  $H_{LAS}$  and  $H_{ec} > 50 \text{ W m}^{-2}$ ).

Title Page	
Abstract	Introduction
Conclusions	References
Tables	Figures
◀	▶
◀	▶
Back	Close
Full Screen / Esc	
Printer-friendly Version	
Interactive Discussion	

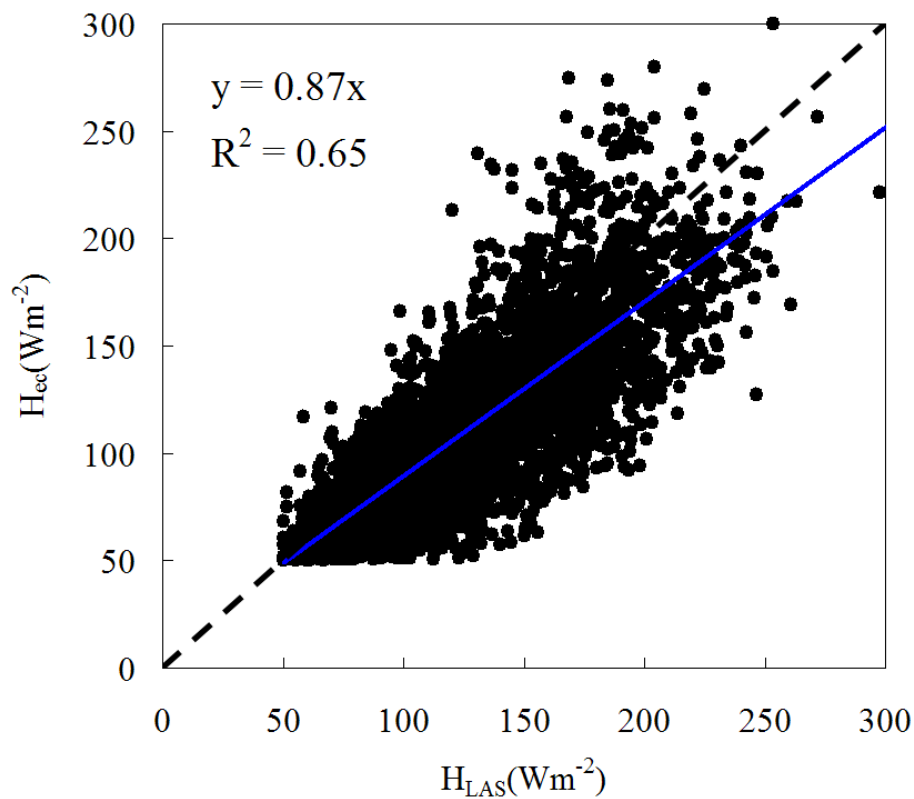


**Fig. 8.** Comparison of  $H_{LAS}$  and  $H_{ec}$  at AR when  $H_{LAS}$  and  $H_{ec} > 50 \text{ W m}^{-2}$  (11 March–31 October 2008, and 1 January–30 June 2009, 30-min averaging time).

Title Page

Abstract

Introduction

Conclusions

References

Tables

Figures

◀

▶

◀

▶

Back

Close

Full Screen / Esc

Printer-friendly Version

Interactive Discussion

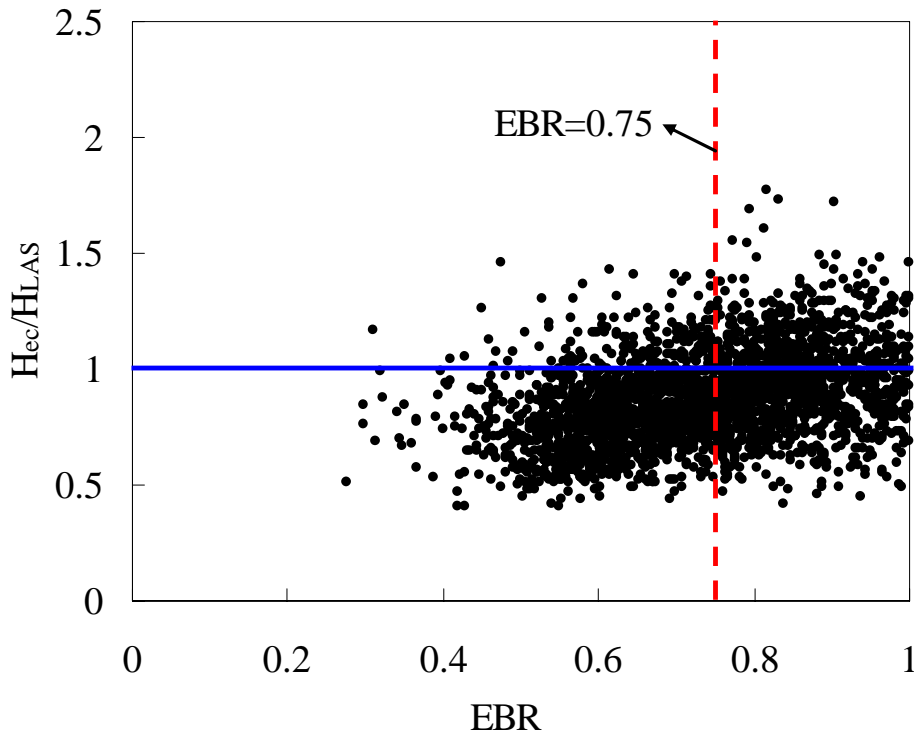


**Fig. 9.**  $H_{ec}/H_{LAS}$  scatters according to Energy Balance closure Ratio (EBR) in 30-min data at AR when  $H_{LAS}$  and  $H_{ec} > 50 \text{ W m}^{-2}$  (11 March–31 October 2008, and 1 January–30 June 2009, 30 min).

## Measurements of energy and water vapor fluxes in the Heihe River Basin

S. Liu et al.

Title Page

Abstract

Introduction

Conclusions

References

Tables

Figures

◀

▶

◀

▶

Back

Close

Full Screen / Esc

Printer-friendly Version

Interactive Discussion



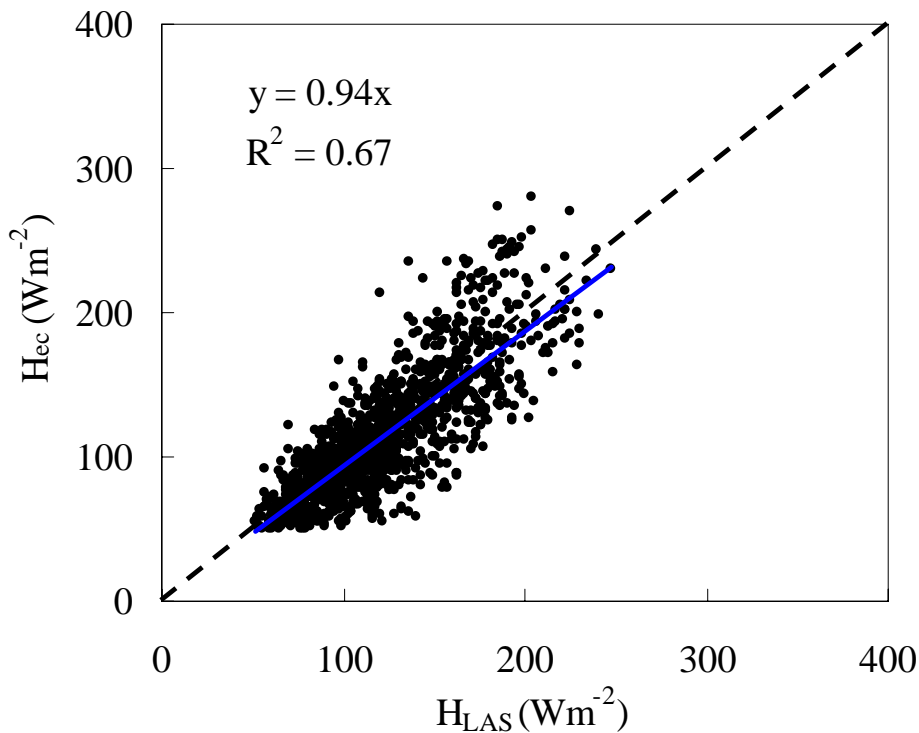


**Fig. 10.** Comparison of  $H_{LAS}$  and  $H_{ec}$  at AR when  $H_{LAS}$  and  $H_{ec} > 50 \text{ W m}^{-2}$  and  $\text{EBR} > 0.75$  (11 March–31 October 2008, and 1 January–30 June 2009, 30-min averaging time).

## Measurements of energy and water vapor fluxes in the Heihe River Basin

S. Liu et al.

<a href="#">Title Page</a>	
<a href="#">Abstract</a>	<a href="#">Introduction</a>
<a href="#">Conclusions</a>	<a href="#">References</a>
<a href="#">Tables</a>	<a href="#">Figures</a>
<a href="#">⏪</a>	<a href="#">⏩</a>
<a href="#">◀</a>	<a href="#">▶</a>
<a href="#">Back</a>	<a href="#">Close</a>
<a href="#">Full Screen / Esc</a>	
<a href="#">Printer-friendly Version</a>	
<a href="#">Interactive Discussion</a>	

